Society of Medical Education & Research

2023, Volume 3, Issue 1, Page No: 139-155

ISSN: 3108-4834

Archive of International Journal of Cancer and Allied Science

Tumor Microenvironment–Induced IFITM3 Activates MET–AKT Signaling to Drive Osimertinib Resistance in EGFR-Mutant NSCLC

Mila Petrovic[1]*, Ana Jovanovic[1]

[1]Department of Oncology, University of Belgrade School of Medicine, Belgrade, Serbia.

***E-mail** ✉ m.petrovic.med@outlook.com

Abstract

Although EGFR-mutant non-small cell lung cancer (NSCLC) initially responds well to osimertinib, a third-generation EGFR tyrosine kinase inhibitor (TKI), acquired resistance to this agent eventually emerges. While several genetic alterations responsible for resistance have been characterized, the molecular factors that drive the onset of such resistance have largely remained elusive.To uncover mediators of osimertinib resistance induction, we examined clinical samples from patients with EGFR-mutant NSCLC and employed cell lines such as PC-9 and H1975. Techniques included transcriptomic profiling and immunohistochemistry of pretreatment tumor samples, spatial transcriptomics, cell viability assays, immunofluorescence and quantitative PCR, RNA sequencing, immunoblotting, mass spectrometry-based comprehensive proteomics, co-immunoprecipitation and proximity ligation assays, as well as a mouse xenograft model.

Transcriptomic evaluation of pretreatment clinical samples revealed that IFITM3 (interferon-induced transmembrane protein 3) was distinctly overexpressed in patients exhibiting a suboptimal response to osimertinib. Immunohistochemical staining verified that individuals whose tumors expressed IFITM3 had significantly shorter progression-free survival during osimertinib therapy. Additional spatial transcriptomics and related experiments demonstrated that IFITM3 levels in cancer cells rose in reaction to cytokines secreted from the tumor microenvironment (TME) under osimertinib exposure. IFITM3 was shown to facilitate osimertinib resistance in NSCLC cell lines by interacting with MET and thereby activating the AKT pathway. Moreover, co-administration of a MET inhibitor prevented the emergence of osimertinib resistance in a mouse xenograft tumor model. The present study identifies cytokine-driven upregulation of IFITM3 in the TME as a novel, previously undescribed mechanism underlying osimertinib resistance. These results indicate that therapeutic targeting of the IFITM3-MET interaction could enhance outcomes of EGFR-TKI therapy in EGFR-mutant NSCLC.

Keywords: IFITM3, MET–AKT signaling, Osimertinib resistance, NSCLC

Introduction

Lung cancer remains the primary cause of cancer-associated mortality globally, with non-small cell lung cancer (NSCLC) accounting for over 80% of cases [1]. EGFR gene mutations occur in approximately 40% of NSCLC in Asian patients and about 10% in those of European ancestry [2, 3]. Osimertinib, a third-generation EGFR-TKI, has demonstrated superior clinical efficacy over prior-generation agents and is now the standard first-line treatment for EGFR-mutated NSCLC [4]. Nevertheless, median progression-free survival with osimertinib is restricted to around 19 months, and roughly one-third of patients acquire resistance within 12 months. Known genetic mechanisms include secondary EGFR mutations and amplification of MET or HER2 [5–8]; however, identifiable genetic changes are absent in nearly half of resistant cases, suggesting important roles for nongenetic processes [9].

Emerging evidence highlights the tumor microenvironment (TME) as a critical contributor to EGFR-TKI resistance [10–14]. In particular, TME-derived cytokines—including tumor necrosis factor-α

Access this article online https://smerpub.com/

Received: 05 February 2023; **Accepted:** 21 May 2023

How to cite this article: Petrovic M, Jovanovic A. Tumor Microenvironment–Induced IFITM3 Activates MET–AKT Signaling to Drive Osimertinib Resistance in EGFR-Mutant NSCLC. Arch Int J Cancer Allied Sci. 2023;3(1):139-55. https://doi.org/10.51847/8A8yWycgNk

(TNF-α), interleukin-6 (IL-6), and interferon-γ (IFN-γ)—have been linked to resistance by altering intracellular signaling in tumor cells [15–18]. Such observations underscore the need for integrated analysis of the TME and malignant cells to pinpoint determinants of osimertinib resistance.

Here, we conducted RNA sequencing of pretreatment clinical specimens from NSCLC patients treated with osimertinib and found that IFITM3 (interferon-induced transmembrane protein 3) was selectively elevated in those with rapid treatment failure. We further elucidated the pathway through which IFITM3 promotes osimertinib resistance and propose MET inhibition as a strategy to overcome resistance in EGFR-mutant NSCLC.

Materials and Methods

Patients and clinical specimens

Clinical data, including progression-free survival on osimertinib, were gathered from 127 patients with EGFR-mutated NSCLC who received osimertinib as first-line monotherapy at eight centers between January 2016 and April 2023. Pretreatment formalin-fixed, paraffin-embedded (FFPE) tumor tissue sections were obtained. For samples suitable for RNA-seq, analysis was conducted on specimens from 10 patients with PFS < 12 months (short PFS group) and 22 patients with PFS > 20 months (long PFS group). The remaining 95 specimens, not used for RNA-seq, underwent immunohistochemistry for IFITM3, with tumor regions verified by hematoxylin-eosin staining. At analysis, disease progression had occurred in 59 of these 95 patients (62.1%) during osimertinib therapy. Post-progression tumor samples were additionally collected from 18 patients who acquired osimertinib resistance and analyzed by immunohistochemistry for IFITM3.

RNA-seq evaluation of pretreatment tumor samples

Tumor material was collected via macrodissection, followed by RNA isolation from two 10-µm-thick FFPE slides (each >1 cm^2 in area) employing the MagMAX FFPE DNA/RNA Ultra Kit (#A31881, Thermo Fisher Scientific). To reverse formaldehyde cross-links, sections underwent 2-h protease digestion at 55 °C and then 1-h heating at 90 °C. Sequencing libraries were built using the Twist Human Core Exome Panel (Twist Biosciences), starting with 100–200 ng RNA input adjusted according to DV200 metrics (fraction of fragments exceeding 200 nucleotides). Indexed precapture libraries underwent 11–16 cycles of amplification for Illumina platforms. Combined libraries were hybridized for 16 h at 70 °C to biotinylated probes, captured on streptavidin beads (Thermo Fisher Scientific), and re-amplified to yield final libraries. Quality checks utilized an Agilent Bioanalyzer, with normalization to 2 nM before loading. Paired-end sequencing was executed on a NovaSeq system (Illumina). Reads were quality-trimmed and adapter-removed via Fastp (version 0.23.4, Bolger AM), aligned to hg38 using HISAT2 (version 2.2.1), and gene counts quantified with FeatureCounts (version 2.0.6). Differential expression, including log2 fold changes and P values, was computed using edgeR (version 4.0, R Bioconductor).

Cell lines and compounds

The study included ten NSCLC lines: five with EGFR-activating alterations (PC-9 [ECACC #90071810], HCC827 [ATCC #CRL-2868], H1975 [ATCC #CRL-5908], H1650 [ATCC #CRL-5883], HCC4006 [ATCC #CRL-2871]) and five EGFR wild-type (A549 [ATCC #CCL-185], H322 [ECACC #95111734], Calu-3 [ATCC #HTB-55], H1437 [ATCC #CRL-5872], H1299 [ATCC #CRL-5803]). Most lines (PC-9, H1975, H1650, HCC827, HCC4006, H322, H1437, H1299) were maintained in RPMI 1640 (Gibco), while A549 and Calu-3 used Dulbecco's modified Eagle's medium (Gibco), all with 10% fetal bovine serum and 1% penicillin-streptomycin (Gibco) under 5% CO_2 at 37 °C in humidified incubators. Drugs including osimertinib (#S7297), MK-2206 (#S1078), capmatinib (#S2788), and methyl-β-cyclodextrin (#S6827) from Selleck Chemicals were solubilized in dimethyl sulfoxide (Fujifilm Wako) and frozen at −20 °C. Infliximab (Mitsubishi Tanabe Pharma, Osaka, Japan) and tocilizumab (Chugai Pharmaceutical, Tokyo, Japan) were also kept at −20 °C. Recombinant cytokines—TNF-α (#210-TA-005, R&D Systems), IFN-γ (#300-02, Peprotech), IL-6 (#206-IL, R&D Systems)—were prepared in 0.1% bovine serum albumin/PBS and stored at −20 °C.

RNA knockdown approaches

For transient knockdown, cells in 96-well plates (Greiner Bio-One) were transfected for 24 h with IFITM3-targeted siRNA (ID s195035, Thermo Fisher Scientific) or nontargeting control (ID 4390843, Thermo Fisher

Scientific) using RNAiMAX (Thermo Fisher Scientific). Stable knockdown in PC-9 and H1975 was achieved via lentiviral delivery of shRNA constructs co-expressing EGFP and puromycin resistance: pLV[shRNA]-EGFP:T2A:Puro-U6 > hIFITM3 (ID VB900080-7459hfw) from VectorBuilder, with scrambled control pLV[shRNA]-EGFP/Puro-U6 > Scramble_shRNA (ID VB010000-0009mxc).

Retroviral overexpression to create stable lines

IFITM3 cDNA originated from H1975 cells. Amplicons were amplified with PrimeSTAR GXL DNA Polymerase (#R050A, Takara Bio) and primers, then cloned into pQCXIP (#639648, Clontech) at NotI/BamHI sites via In-Fusion HD Cloning Kit (#639648, Takara Bio), yielding pQCXIP-IFITM3. A Flag-tagged variant (pQCXIP-Flag-IFITM3) was made similarly. Vectors (or empty control [EV]) were packaged in HEK293T cells (ATCC #CRL-1573) using Retrovirus Packaging Kit Ampho (#6161, Takara Bio) and Lipofectamine 3000 (Invitrogen). Viral supernatant was 0.45-µm filtered, concentrated overnight at 4 °C with Retro-X Concentrator (Clontech), and pelleted at 1500 × g for 45 min at 4 °C. Target PC-9 or H1975 cells were infected 24 h with virus plus 8 µg/ml polybrene (Nacalai Tesque), recovered 24 h, and selected in 2 µg/ml puromycin (Invitrogen). Lines were denoted PC-9/EV, H1975/EV, PC-9/IFITM3, H1975/IFITM3, and PC-9/Flag-IFITM3.

Assessment of cell proliferation

3000 cells/well were plated in 96-well flat-bottom dishes (Greiner Bio-One), grown 24 h at 37 °C/5% CO_2, treated 72 h with agents, then incubated 2 h with 10 µl Cell Counting Kit 8 (Nacalai Tesque). Optical density at 450 nm was read on a Multiskan FC device (Thermo Fisher Scientific).

Generation of resistant sublines

To develop resistance, 1.2×10^5 cells/well of PC-9/EV, PC-9/IFITM3, H1975/EV, or H1975/IFITM3 were cultured in six-well plates (Greiner Bio-One) and subjected to stepwise osimertinib escalation from 10 nM to 1 µM over ≤30 days, advancing doses at 70% confluence.

Mass spectrometry-based interactome profiling

Quantitative proteomics employed label-free LC-MS/MS. Peptides were fractionated on a NANO HPLC Capillary Column (Nikkyo Technos) via 90-min 5–95% acetonitrile gradient at 500 nl/min. Detection occurred on Orbitrap Exploris 240 (Thermo Fisher Scientific) with nano-electrospray in data-dependent mode: full scans at 60,000 resolution, top 10 precursors fragmented (30% energy, 1.6-m/z window, dynamic exclusion). Spectra were processed in Proteome Discoverer 3.0 (Thermo Fisher Scientific). Interactome candidates required ≥5-fold enrichment in anti-IFITM3 versus control IgG pulldowns, with $P < 0.05$.

Western blot examination

Cells underwent rinsing in chilled PBS prior to disruption in RIPA lysis buffer (Thermo Fisher Scientific) supplemented with protease and phosphatase inhibitor cocktails (Nacalai Tesque). Resulting extracts were resolved on 10% SDS-polyacrylamide gels, followed by electrotransfer onto polyvinylidene difluoride membranes. Membranes received overnight incubation at 4 °C with primary antibodies directed against IFITM3 (#59212), phospho-EGFR (#3777), EGFR (#4267), phospho-ERK1/2 (#4370), ERK1/2 (#9102), phospho-AKT (#9271), AKT (#9272), DYKDDDDK Flag tag (#14793), phospho-MET (#3077), MET (#8198), phospho-GSK3β (#9323), GSK3β (#9315), phospho-mTOR (#5536), mTOR (#2983), or β-actin (#4970), each sourced from Cell Signaling Technology and applied at 1:1000 dilution. Subsequent 1-h room-temperature exposure to horseradish peroxidase-linked anti-rabbit IgG secondary antibodies (1:10,000; #NA9340, Cytiva) enabled chemiluminescent detection via Pierce ECL Plus Substrate (Thermo Fisher Scientific), with signal capture on a ChemiDoc Touch MP imager (Bio-Rad). Band intensities per lane were measured using Image Lab software (Bio-Rad) and standardized against β-actin levels. All displayed blots originated from identical experimental runs and underwent simultaneous processing.

Co-immunoprecipitation preceding LC-MS/MS or western blot

Cellular disruption occurred in Pierce IP Lysis Buffer (#87787, Thermo Fisher Scientific), followed by 15-min centrifugation at 15,000 × g and 4 °C. Cleared supernatants underwent overnight rotation at 4 °C with anti-IFITM3 antibodies (#59212, Cell Signaling Technology), normal rabbit IgG control (#2729, Cell Signaling Technology), or anti-Flag antibodies (#14793, Cell Signaling Technology), combined with magnetic protein A/G beads (Pierce). Captured complexes

received Tris-buffered saline washes before resuspension in low-pH Pierce IgG Elution Buffer (#21028, Thermo Fisher Scientific; pH 2.0) for downstream proteomics or immunoblotting.

Immunohistochemical detection of IFITM3

Neoplastic tissues were preserved in 10% neutral buffered formalin to generate FFPE blocks. 3-µm sections underwent immunohistochemistry according to established protocols [19]. Antigen unmasking employed Immunosaver (Nissin EM), followed by overnight 4 °C exposure to rabbit monoclonal anti-IFITM3 (#59212, Cell Signaling Technology). Visualization relied on Histofine Simple Stain MAX-PO (M) (Nichirei Bioscience) and diaminobenzidine substrate (Histofine DAB, Nichirei Bioscience). Evaluation focused exclusively on tumor cell staining, categorized as positive or negative by a qualified pathologist. IFITM3 scoring criteria were: 0 (<1% positive neoplastic cells), 1 (1–10%), 2 (10–50%), and 3 (>50%).

Transcriptomic profiling of NSCLC lines

Total RNA from PC-9 cells harboring stable IFITM3 or control shRNAs was purified using RNeasy Mini Kit (#74016, Qiagen), with three independent replicates per group. RNA yield and integrity were verified via NanoDrop-2000 (Thermo Fisher Scientific) and 2200 TapeStation (Agilent Technologies). Ribosomal RNA depletion preceded library preparation with the MGI Easy rRNA Depletion Kit and the MGI Easy RNA Directional Library Prep Set (both MGI). Paired-end 150-bp sequencing occurred on the NovaSeq platform. Read trimming for quality and adapters utilized Fastp (version 0.23.4), alignment to hg38 employed HISAT2 (version 2.2.1), and gene quantification relied on FeatureCounts (version 2.0.6). Pathway enrichment assessment was executed via Metascape [20].

Visium-based spatial gene expression in patient samples

Processing and cluster annotation followed prior methodologies [21]. Eight FFPE tumor blocks were examined, comprising paired pre- and post-osimertinib specimens from two EGFR-mutant NSCLC cases plus four additional baseline samples. Analysis utilized 10X Genomics Visium HD. Deparaffinized sections received hematoxylin-eosin staining and imaging on the Evident VS200 microscope. Samples required DV200 ≥ 30%. Library construction adhered to 10X Genomics guidelines, with quality verification before 150-bp paired-end sequencing on NovaSeq X Plus. Data alignment and spatial mapping were employed with Space Ranger (v3.0.0). Clustering mirrored single-cell workflows in Scanpy, excluding poor-quality features, correcting batch variation via Harmony, and applying the Leiden algorithm (resolution 0.4) to yield 18 clusters annotated as epithelial, stromal, or immune based on canonical markers. Refined subclustering incorporated inferCNVpy for malignant versus non-malignant epithelial discrimination.

Quantitative reverse transcription PCR

Cellular RNA isolation used the RNeasy Mini Kit (Qiagen), with cDNA synthesis via PrimeScript RT Reagent Kit (#RR037A, Takara Bio). Amplification employed SYBR Green PCR Master Mix (#4344463, Thermo Fisher Scientific) and target-specific primers. IFITM3 levels were calculated by $2^{-\Delta\Delta Ct}$ approach, referenced to GAPDH.

Fluorescent detection of IFITM3 localization

PC-9 cultures at 70% density on 12-mm coverslips (Matsunami) in 24-well dishes (Corning) received 15-min fixation in 4% paraformaldehyde/PBS and 10-min permeabilization in 0.3% Triton X-100/PBS. Overnight 4 °C incubation applied Alexa Fluor 488-labeled anti-IFITM3 (1:500), prepared by conjugating #59212 antibody (Cell Signaling Technology) using FlexAble CoraLite Plus 488 Kit (#KFA001, Proteintech). Additional overnight 4 °C staining used Alexa Fluor 594-phalloidin (#ab176757, Abcam). Capture occurred on the BZX800 microscope (Keyence). Z-stack compilation into full-focus projections employed BZ-H4A software (Keyence). IFITM3 puncta counting across ≥50 cells in nine fields utilized BZ-X Analyzer (BZ-H4A, Keyence).

Duolink proximity ligation for protein interaction

PC-9/EV and PC-9/IFITM3 cultures at 70% confluence on 12-mm coverslips underwent fixation and permeabilization as above. Overnight 4 °C primary incubation combined with mouse anti-IFITM3 (#2524, Cell Signaling Technology) and rabbit anti-MET (#8242, Cell Signaling Technology) at 1:500 for Duolink PLA Fluorescence detection (#DUO92002 and #DUO92004, Sigma-Aldrich). Further overnight 4 °C anti-E-cadherin (#AF648, R&D Systems) staining preceded 1-h room-temperature Alexa Fluor 488 anti-goat secondary (#A11055, Invitrogen). Signal acquisition and quantification mirrored immunofluorescence procedures.

Animal experiments

Female athymic mice aged four weeks were sourced from CLEA Japan. Either PC-9/EV or PC-9/IFITM3 cells (5.0×10^6) were administered subcutaneously into the mouse flank. Seven days post-injection, animals were randomly assigned to the groups outlined in **Figure 6**. Tumor size was assessed biweekly, with volume determined by the equation: (length × width × width)/2. Euthanasia via cervical dislocation under anesthesia (medetomidine, midazolam, and butorphanol combination) occurred when tumors exceeded 2000 mm^3 or at 28 days following treatment initiation.

Data analysis

Results are expressed as means ± s.e.m. (unless specified otherwise) and were evaluated using Fisher's exact test or one-way ANOVA with Tukey's post-test via GraphPad Prism 10. The ideal threshold for IFITM3 positivity was established through model selection metrics, including Corrected Akaike Information Criterion (AICc) and Bayesian Information Criterion (BIC), employing JMP 17 software. Survival curves (Kaplan-Meier) and log-rank comparisons were also conducted in JMP 17. Statistical significance was set at $P < 0.05$.

Findings

Elevated IFITM3 levels correlate with reduced osimertinib effectiveness in EGFR-mutant NSCLC

Clinical records and FFPE tumor blocks from 127 EGFR-mutant NSCLC cases treated with first-line osimertinib monotherapy (January 2016–April 2023, eight centers) were reviewed. Short PFS was designated as <12 months and long PFS as >20 months, guided by prior osimertinib trial outcomes [4]. RNA-seq was conducted on 32 cases with adequate RNA: 10 short PFS and 22 long PFS, forming the discovery set **(Figure 1a)**. The other 95 cases comprised the validation set, examined via IHC **(Figure 1a)**. Discovery cohort RNA-seq yielded robust data, with high gene detection and mapping rates (>80% overall, >90% in most) plus consistent expression profiles. Differential analysis across >19,000 genes pinpointed IFITM3 as the sole markedly overexpressed transcript in short-PFS cases **(Figure 1b)**. High IFITM3 cases displayed reduced PFS and lower response rates to osimertinib versus low-expressors **(Figures 1c and 1d)**. Validation through IHC on 95 specimens **(Figures 1e–1h)** involved testing cutoffs of 1%, 10%, and 50% positive tumor cells; model criteria (AICc, BIC) favored 10%. IFITM3-positive tumors showed markedly shorter PFS (median 18.4 vs. 24.8 months; HR 1.87, 95% CI 1.06–3.30; P = 0.013) compared to negative ones **(Figure 1f)**.

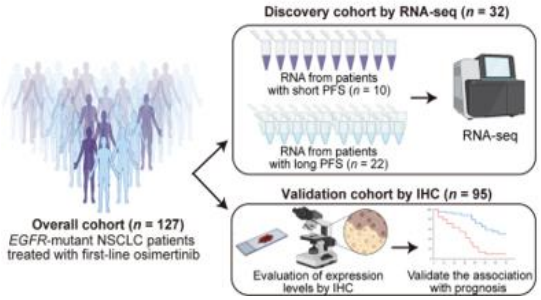

a)

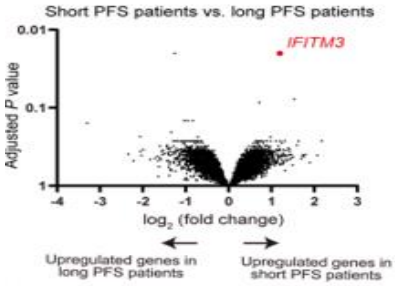

b)

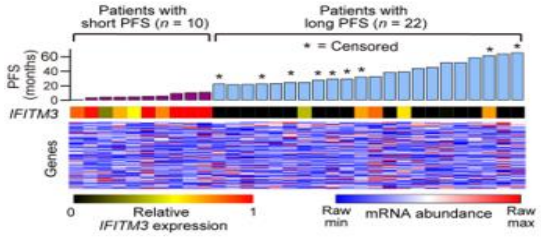

c)

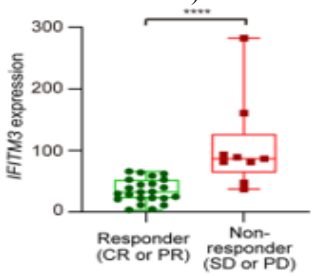

d)

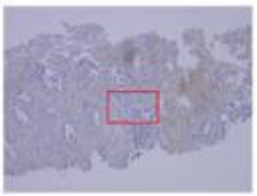

e)

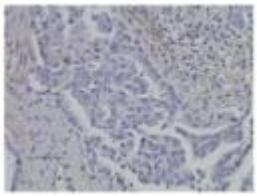

f)

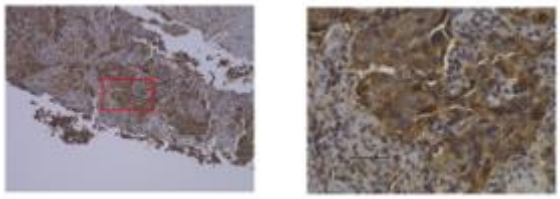

g) h)

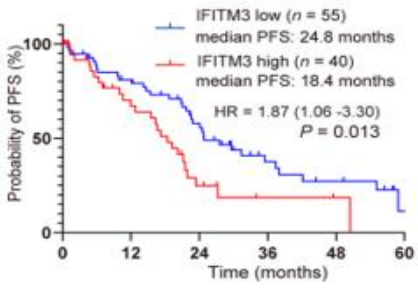

i)

Figure 1. Elevated IFITM3 correlates with unfavorable outcomes in EGFR-mutant NSCLC. a Study outline. Total first-line osimertinib-treated EGFR-mutated cohort (n = 127) split into discovery (n = 32, RNA-seq) and validation (n = 95, IHC) arms. Discovery compared short PFS (<12 months, n = 10) versus long PFS (>20 months, n = 22). b Volcano display of expression differences (short vs. long PFS). Red upper-right point denotes upregulation in short PFS (adjusted P < 0.05, log2 fold change >1). c Heatmap depicting IFITM3 and select genes across 32 discovery patients ordered by increasing PFS; bar indicates PFS duration, asterisks mark censored cases. d IFITM3 transcript levels by response category in the discovery set. Responders: CR/PR; nonresponders: SD/PD. ****P < 0.0001 (one-way ANOVA, Tukey's). e–h Low (e-g) and high (f-h) power IHC views of IFITM3 in low (e-f) versus high (g-h) expressing tumors. Scale bars, 50 µm. i Kaplan-Meier PFS curves by IFITM3 status in the validation set.

IFITM3 contributes to osimertinib resistance in EGFR-mutant NSCLC models

Western blotting indicated greater IFITM3 protein in EGFR-mutated (L858R or exon-19 deletion) NSCLC lines compared to EGFR wild-type counterparts **(Figure 2a)**. Mining CCLE data from 1156 solid tumor lines [22] confirmed higher IFITM3 transcripts in EGFR driver-mutant lines versus wild-type or other EGFR variants **(Figure 2b)**. TCGA advanced lung adenocarcinoma samples similarly revealed increased IFITM3 in EGFR driver-mutant tumors over wild-type **(Figure 2c)**. These observations link IFITM3 to active EGFR signaling, implying greater relevance in driver-mutant contexts. Functional studies in EGFR-mutant lines showed that transient siRNA depletion of IFITM3 markedly enhanced osimertinib-induced viability loss versus single interventions **(Figure 2d)**. Stable shRNA-mediated IFITM3 reduction heightened osimertinib potency **(Figures 2e and 2f)**, while ectopic IFITM3 overexpression diminished it **(Figures 2g and 2h)**. Chronic osimertinib challenge demonstrated that IFITM3-overexpressing cells acquired tolerance to 1 µM drug within 30 days, unlike controls **(Figures 2i and 2j)**.

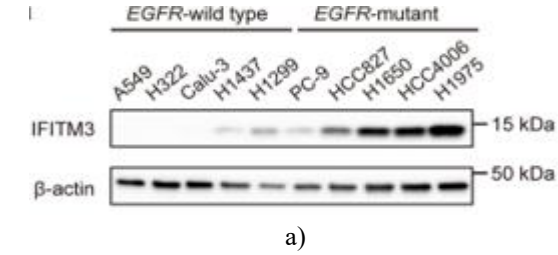

a)

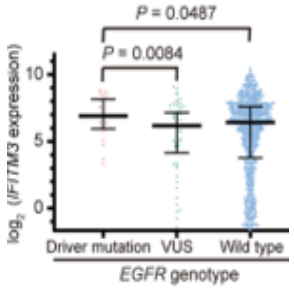

b)

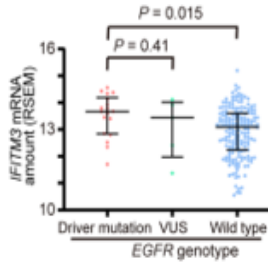

c)

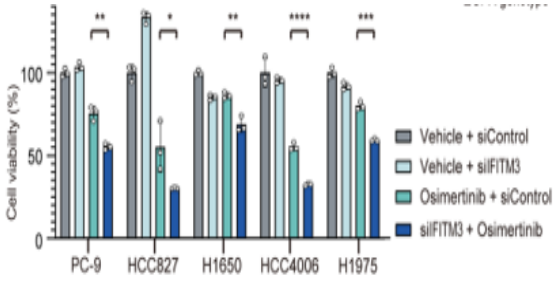

d)

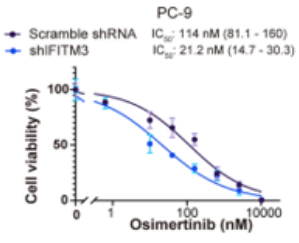

e)

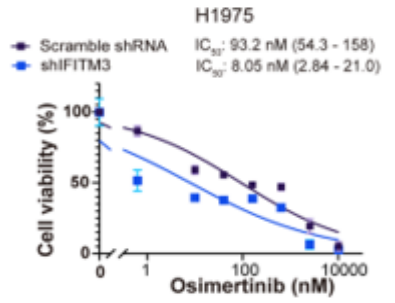

f)

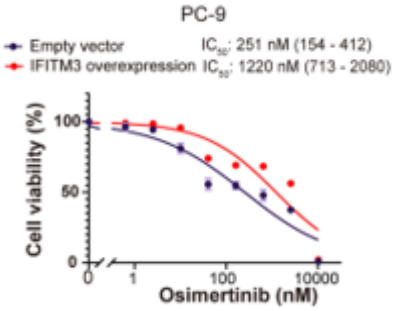

g)

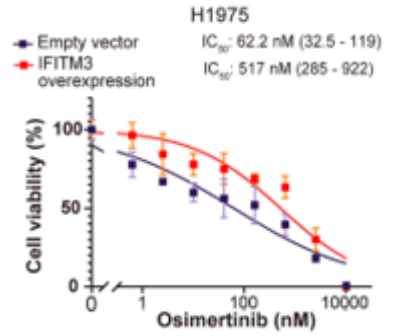

h)

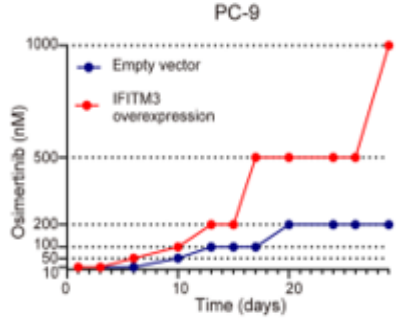

i)

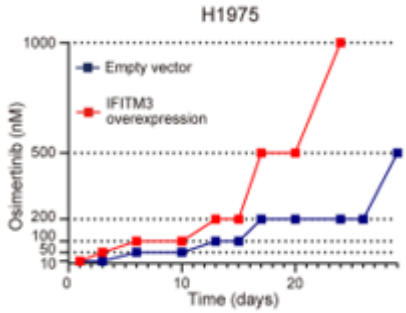

j)

Figure 2. Elevated IFITM3 levels promote osimertinib resistance and reduce drug sensitivity. a Western blot detection of IFITM3 and β-actin (loading control) across EGFR wild-type and EGFR-mutant NSCLC lines. b,c IFITM3 transcript levels grouped by EGFR status in 1156 solid-tumor lines from CCLE (b) and 199 stage III–IV lung adenocarcinoma cases from TCGA (c). VUS, variant of uncertain significance; RSEM, RNA-seq by Expectation-Maximization. Bars show median with 95% CI. P values from one-way ANOVA with Tukey's test. d Cell viability (colorimetric) in EGFR-mutant NSCLC lines after transfection with control or IFITM3 siRNA and 72-h exposure to 100 nM osimertinib or vehicle. *P < 0.05, **P < 0.01, ***P < 0.001, ****P < 0.0001 (one-way ANOVA, Tukey's). e-f Viability of PC-9 (e) and H1975 (f) cells with stable IFITM3 or scrambled shRNA after 72-h osimertinib at the indicated doses. g-h Viability of PC-9 (g) and H1975 (h) cells stably overexpressing IFITM3 or empty vector after 72-h osimertinib exposure. i-j Timeline of resistance acquisition in PC-9 (i) and H1975 (j) cells overexpressing IFITM3 versus empty vector controls. Osimertinib dose escalated from 10 nM to 1 µM whenever cultures reached 70% confluence; doses marked on the y-axis. Data in d–h represent means ± s.e.m. from triplicates of one experiment, typical of three independent runs. IC50 values with 95% CI are shown in e–h. Data in i–j are from one of two independent experiments performed without replicates.

IFITM3 levels rise following osimertinib exposure

Using previously generated spatial transcriptomics data from EGFR-mutant NSCLC samples collected before treatment and after resistance emergence [21], we examined IFITM3 and its regulators in the tumor microenvironment for two patients: one with short PFS

(6 months) and one with long PFS (36 months). Clustering and hematoxylin-eosin staining distinguished tumor cells, macrophages, fibroblasts, T cells, and B cells **(Figure 3a)**. Tumor cells exhibited the highest IFITM3 expression of all clusters **(Figure 3b)**. Pretreatment tumor-cell IFITM3 was markedly higher in the short-PFS patient than in the long-PFS patient **(Figures 3a and 3c)**, aligning with our RNA-seq and IHC results. Notably, IFITM3 increased in posttreatment samples compared with pretreatment samples in both patients **(Figures 3a and 3c)**. Immunohistochemistry on 95 pretreatment validation-cohort specimens versus 18 post-progression specimens confirmed significantly greater IFITM3 protein in the latter group. These observations indicate that osimertinib therapy triggers IFITM3 upregulation in malignant cells.

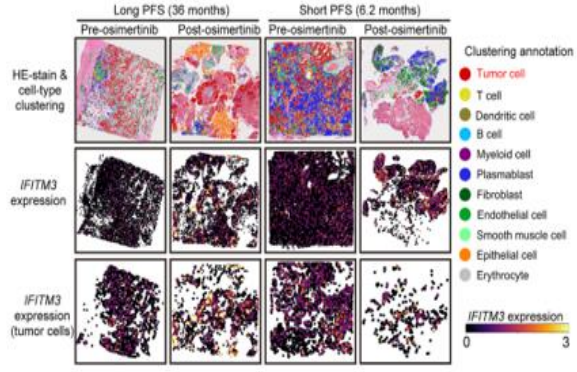

a)

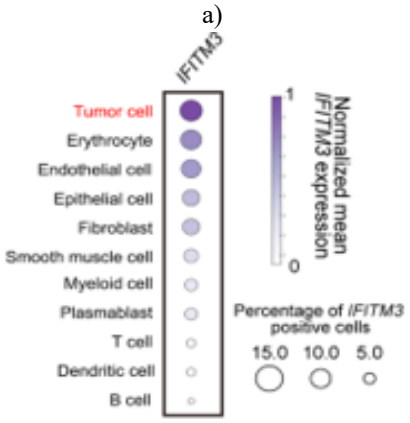

b)

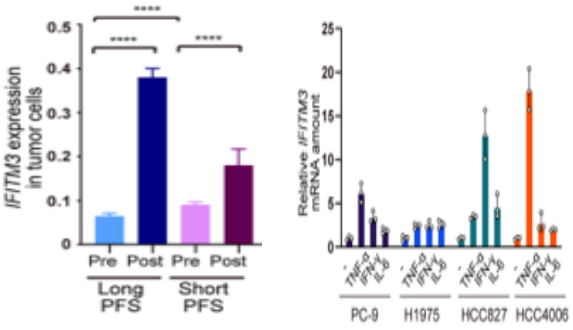

c) g)

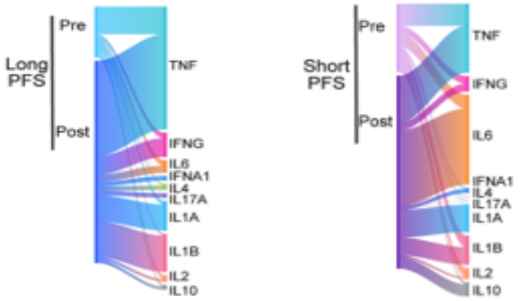

d) e)

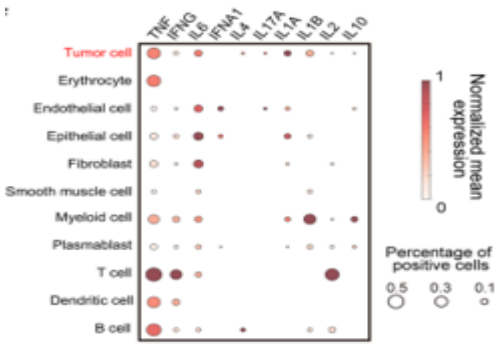

f)

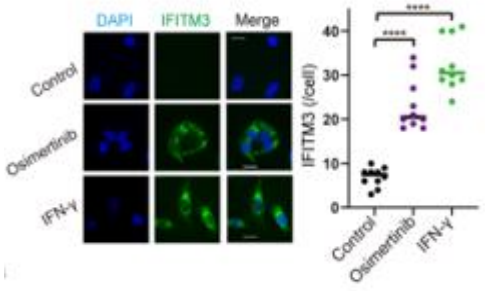

h)

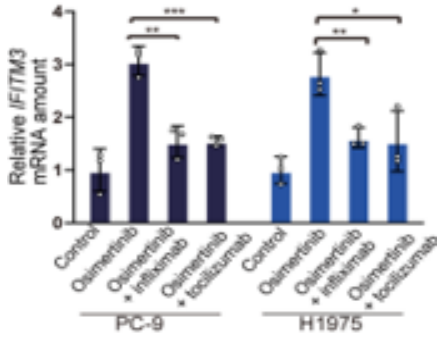

i)

Figure 3. Cytokines from the tumor microenvironment drive IFITM3 induction during osimertinib therapy. a–f Spatial transcriptomics of pre- and post-osimertinib tumor samples from two EGFR-mutant NSCLC patients (one long PFS, one short PFS) [21]. a Hematoxylin-eosin images and cluster maps (top), IFITM3 across all cells (middle), IFITM3 in tumor cells only (bottom). b IFITM3 levels and positive-cell counts by cell type. c Tumor-cell IFITM3 before and after resistance in long- and short-PFS cases. Bars show median and 95% CI. d-e Sankey plots of cytokine-gene expression in cells adjacent to tumor cells pre- and post-treatment for long-PFS (d) and short-PFS (e) patients. f Bubble chart displaying cytokine-gene expression and positive-cell numbers across cell types. g RT-qPCR measurement of IFITM3 mRNA in EGFR-mutant NSCLC lines after 24-h incubation with TNF-α (10 ng/ml), IL-6 (10 ng/ml), IFN-γ (50 ng/ml), or no cytokine. h Immunofluorescence of IFITM3 (green) in PC-9 cells after 24-h exposure to osimertinib (100 nM) or IFN-γ (50 ng/ml). Nuclei counterstained with DAPI (blue). Images are optical sections. Scale bars, 20 μm. IFITM3 puncta quantified per cell (n = 9 fields, ≥50 cells total). Bars indicate median. i RT-qPCR of IFITM3 mRNA in PC-9 and H1975 cells treated 24 h with or without osimertinib (100 nM) plus anti-TNF-α (infliximab, 1 μg/ml) or anti-IL-6R (tocilizumab, 10 μg/ml). Data in g and i are means ± s.e.m. from triplicates of one experiment, representative of two independent runs. *P < 0.05, **P < 0.01, ***P < 0.001, ****P < 0.0001 (one-way ANOVA, Tukey's).

Osimertinib triggers cytokine-mediated IFITM3 upregulation

Since cytokines are known to boost IFITM3 [23, 24], we interrogated cytokine-gene expression in cells neighboring tumor cells within the spatial transcriptomics dataset. Genes encoding TNF-α, IL-6, and IFN-γ were strongly elevated posttreatment versus pretreatment in both patients **(Figures 3d and 3e)**. Pretreatment cytokine-gene expression in peritumoral cells was also higher in the short-PFS patient than in the long-PFS patient. Although mainly expressed by microenvironmental cells, these cytokines were detectable in tumor cells as well **(Figure 3f)**. RT-qPCR validated that TNF-α, IL-6, IFN-γ, or osimertinib exposure raised IFITM3 mRNA in EGFR-mutant lines **(Figure 3g)**. Immunofluorescence confirmed increased IFITM3 protein in PC-9 cells after osimertinib or cytokine treatment, with partial membrane localization **(Figure 3h)**. Blocking IL-6R or TNF-α with antibodies prevented the osimertinib-induced IFITM3 rise **(Figure 3i)**, demonstrating cytokine dependence. To explore whether surrounding cell composition differed near IFITM3-positive versus negative tumor cells, we expanded spatial analysis to eight samples (four new pretreatment plus the original four). IFITM3 varied across tumor regions **(Figure 3a)**, yielding 14,698 positive and 112,490 negative tumor cells. Examination of the 50 nearest neighbors to each tumor cell revealed no significant differences in microenvironmental cell-type proportions based on tumor-cell IFITM3 status.

IFITM3-driven osimertinib resistance involves PI3K-AKT pathway stimulation

To uncover how IFITM3 diminishes tumor-cell responsiveness to osimertinib, we conducted RNA-seq on PC-9 cells with stable IFITM3 shRNA depletion versus matched controls. IFITM3 reduction led to lowered expression of proliferation-related genes including TOP2A and MKI67 **(Figure 4a)**. GSEA indicated substantial suppression of gene sets linked to unfavorable lung cancer prognosis **(Figure 4b)**. KEGG enrichment highlighted major alterations in oncogenic pathways, with the phosphatidylinositol 3-kinase (PI3K)–AKT cascade showing prominent involvement **(Figure 4c)**. Supporting this, western blotting demonstrated elevated AKT phosphorylation in EGFR-mutant lines with forced IFITM3 expression, even under osimertinib challenge **(Figure 4d)**. In contrast, transient IFITM3 siRNA depletion lowered AKT activation and subsequently reduced phosphorylation of its downstream target GSK3β **(Figure 4e)**. Although the AKT blocker MK-2206 by itself minimally impacted viability, it effectively reinstated osimertinib potency in IFITM3-

overexpressing lines **(Figures 4f and 4g)**. Collectively, these data establish that IFITM3 confers osimertinib resistance primarily through PI3K-AKT pathway engagement.

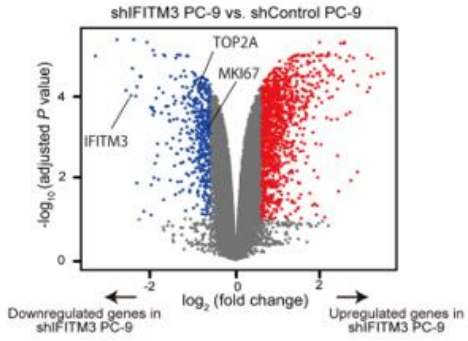

a)

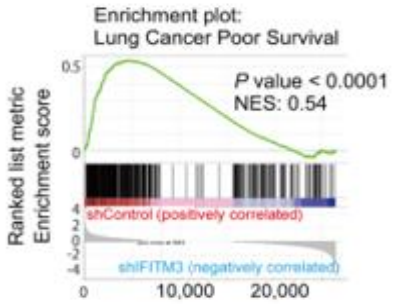

b)

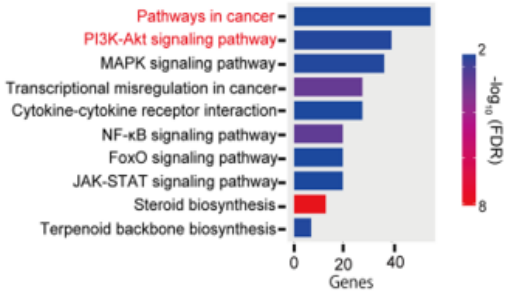

c)

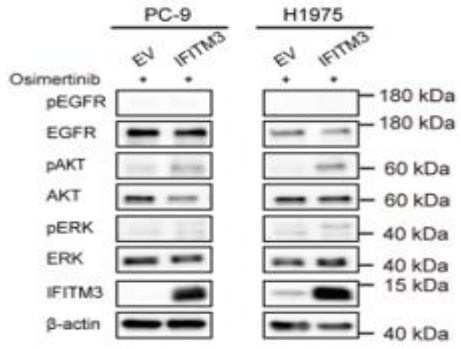

d)

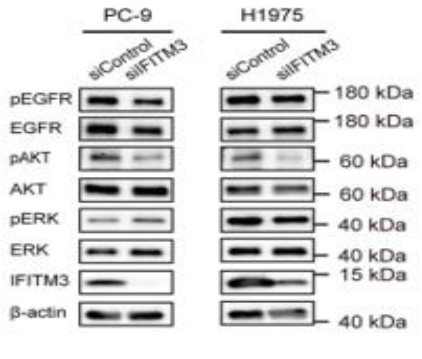

e)

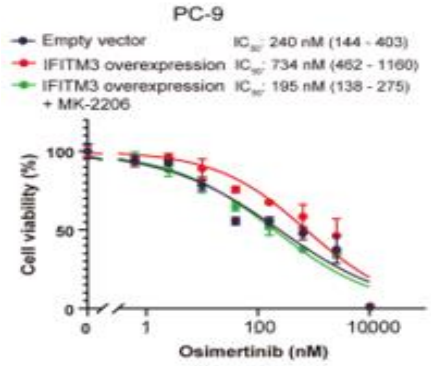

f)

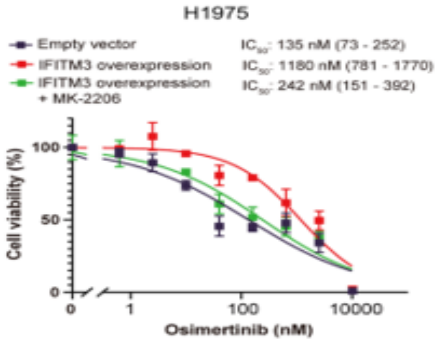

g)

Figure 4. IFITM3 impairs osimertinib efficacy by engaging the PI3K-AKT cascade. a Volcano display of RNA-seq differential expression in PC-9 cells with stable IFITM3 shRNA versus control shRNA (n = 3 replicates). Red/blue points mark upregulated/downregulated transcripts in knockdown cells (adjusted $P < 0.05$, log2 fold change >1 or <–1). b GSEA results for the Lung Cancer Poor Survival signature. NES, normalized enrichment score. c KEGG enrichment for downregulated genes from RNA-seq, ordered by gene count and shaded by $-\log_{10}$(FDR). d Western blot of total and phosphorylated EGFR, AKT, ERK, plus IFITM3 in PC-9 and H1975 cells overexpressing IFITM3 or

empty vector (EV), treated 24 h with 100 nM osimertinib. e Western blot of total/phosphorylated EGFR, AKT, ERK, and IFITM3 in PC-9/H1975 cells with control or IFITM3 siRNA (no osimertinib). f-g Viability of PC-9/IFITM3 versus PC-9/EV (f) and H1975/IFITM3 versus H1975/EV (g) after 72-h exposure to graded osimertinib ± MK-2206 (500 nM). Data in f–g are means ± s.e.m. from triplicates of one experiment, typical of three runs. IC50 with 95% CI provided.

IFITM3 promotes osimertinib resistance via MET-dependent AKT stimulation

To determine how IFITM3 engages the PI3K-AKT axis, we carried out co-immunoprecipitation using anti-IFITM3 antibodies in PC-9 and H1975 cells, followed by label-free LC-MS/MS proteomics on bound proteins. This yielded 546 candidate interactors in PC-9 and 253 in H1975, with 97 overlapping across both lines **(Figure 5a)**. Among these common partners, 58 were membrane-localized, and MET stood out as the sole receptor tyrosine kinase connected to PI3K-AKT signaling **(Figure 5a)**. Anti-Flag co-immunoprecipitation in Flag-IFITM3-expressing PC-9 cells verified direct IFITM3–MET association **(Figure 5b)**. Proximity ligation assay detected markedly more IFITM3–MET proximity signals in IFITM3-overexpressing cells than controls **(Figures 5c and 5d)**. Stable IFITM3 depletion in PC-9 reduced both MET and AKT phosphorylation **(Figure 5e)**. These results point to IFITM3 activating AKT through physical interaction with MET. Testing MET blockade, capmatinib monotherapy minimally affected viability but effectively resensitized IFITM3-overexpressing cells to osimertinib **(Figures 5f and 5g)**. Considering prior evidence that IFITM3 maintains lipid raft integrity [25], we probed raft involvement: the raft disruptor methyl-β-cyclodextrin abrogated IFITM3-driven MET phosphorylation elevation, reversed osimertinib resistance, and had negligible standalone toxicity, indicating lipid rafts support IFITM3-mediated MET engagement.

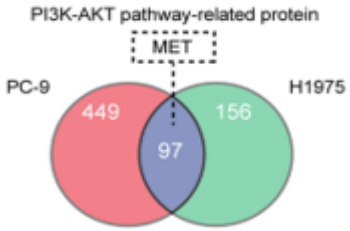

a)

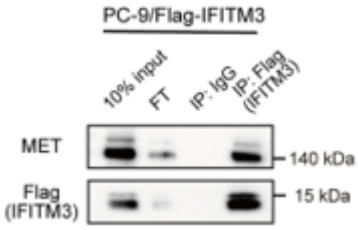

b)

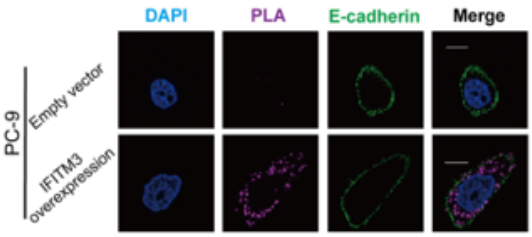

c)

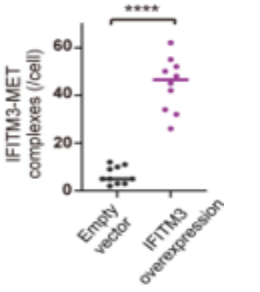

d)

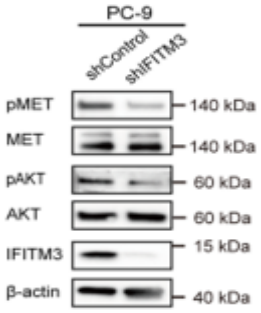

e)

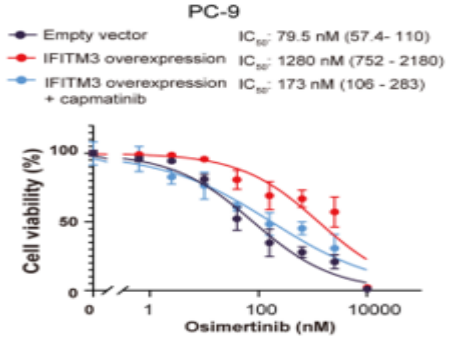

f)

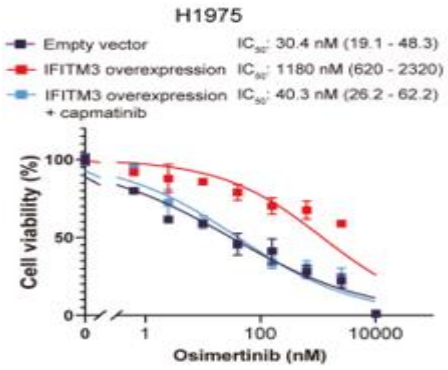

g)

Figure 5. IFITM3 engages MET to stimulate AKT signaling. a Venn representation of overlapping proteins detected as candidate IFITM3 interactors via LC-MS/MS of anti-IFITM3 immunoprecipitates from PC-9 and H1975 cells. b Co-immunoprecipitation using anti-Flag (or control IgG) in PC-9 cells with stable Flag-IFITM3 expression. Immunoblots of immunoprecipitates (IP), 10% input lysates, and flow-through (FT) probed for MET and Flag. c Fluorescence micrographs showing IFITM3–MET proximity signals (purple) via in situ PLA in PC-9/EV and PC-9/IFITM3 cells. E-cadherin staining (green) and DAPI nuclear counterstain (blue). Images acquired by optical sectioning. Scale bars, 10 µm. d Quantification of IFITM3–MET signals per cell as in c (n = 10 fields, ≥50 cells total). Bars show median. ****P < 0.0001 (one-way ANOVA, Tukey's). e Western blot of total and phosphorylated MET, AKT, plus IFITM3 in PC-9 cells with IFITM3 or control shRNA. f-g Viability of PC-9/EV versus PC-9/IFITM3 (f) and H1975/EV versus H1975/IFITM3 (g) after 72-h treatment with graded osimertinib ± capmatinib (100 nM). Data in f–g are means ± s.e.m. from triplicates of one experiment, typical of three runs. IC50 with 95% CI provided.

Blocking MET prevents IFITM3-driven osimertinib resistance in vivo

To confirm results in a living system, we generated subcutaneous xenografts in nude mice using PC-9/IFITM3 cells **(Figure 6a)**. Tumors from empty-vector PC-9/EV cells remained responsive to osimertinib, whereas PC-9/IFITM3-derived tumors quickly became refractory **(Figures 6b and 6cc)**. Adding capmatinib to osimertinib effectively controlled the growth of these resistant PC-9/IFITM3 tumors **(Figures 6d and 6e)**, without causing ≥10% body weight reduction in any animals. These observations demonstrate that MET blockade can overcome IFITM3-associated osimertinib resistance.

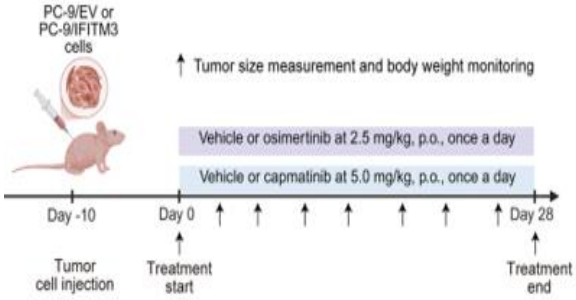

a)

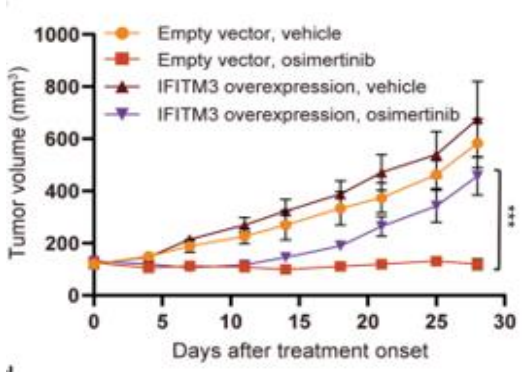

b)

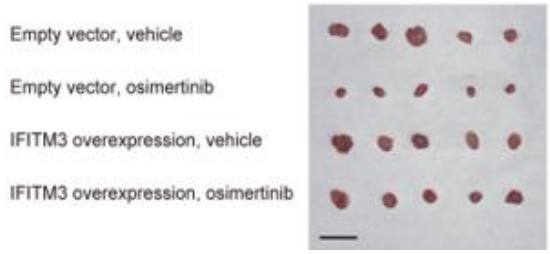

c)

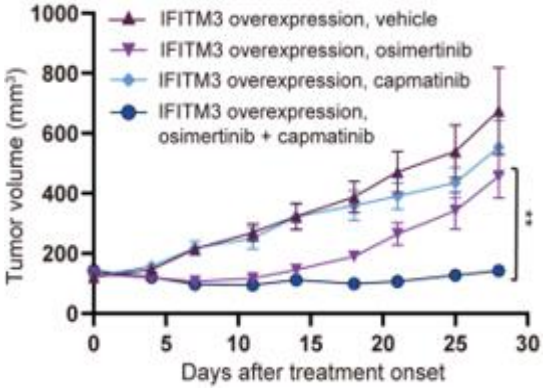

d)

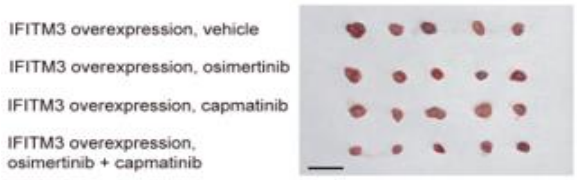

e)

Figure 6. MET-targeted therapy halts IFITM3-linked osimertinib resistance in xenografts. a Experimental timeline. PC-9/EV or PC-9/IFITM3 cells were injected subcutaneously on day −10. Daily oral dosing started on day 0 with vehicle/osimertinib (2.5 mg/kg) or vehicle/capmatinib (5.0 mg/kg). Euthanasia at day 28. b Growth curves of PC-9/EV and PC-9/IFITM3 tumors under vehicle or osimertinib. c Excised tumors from b at day 28. Scale bar, 20 mm. d Growth curves of PC-9/IFITM3 tumors under vehicle, osimertinib, or combined capmatinib. e Excised tumors from d at day 28. Scale bar, 20 mm. Data are means ± s.e.m. (n = 5 mice/group). **P < 0.01, ***P < 0.001 (one-way ANOVA, Tukey's).

IFITM3, a compact membrane protein induced by multiple cytokines [26–28], has been linked to cancer advancement and therapeutic failure [29–31]. Its involvement in EGFR-TKI resistance, however, remained unexplored. Here, we establish that IFITM3 binds MET to sustain PI3K-AKT activation, thereby fostering osimertinib resistance. Cytokines secreted by microenvironmental cells and by tumor cells themselves elevate IFITM3 levels during osimertinib exposure. This heightened IFITM3 maintains AKT phosphorylation despite EGFR inhibition, supporting malignant cell persistence **(Figure 7)**.

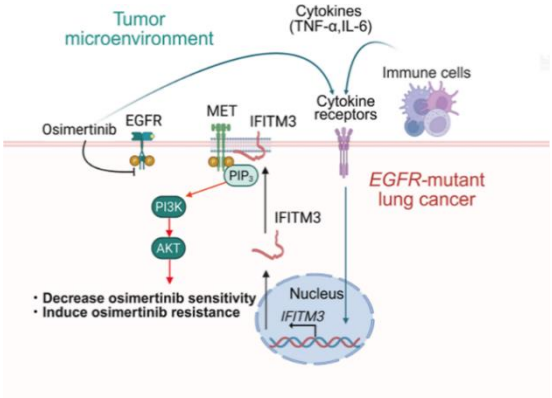

Figure 7. Model of IFITM3-dependent osimertinib resistance in EGFR-mutant NSCLC.

Microenvironmental immune and stromal cells release cytokines that boost IFITM3 in cancer cells under osimertinib pressure. Tumor cells also produce cytokines, amplifying IFITM3 induction. Elevated IFITM3 binds MET, driving PI3K-AKT signaling and diminishing osimertinib efficacy, culminating in resistance. PIP3, phosphatidylinositol 3,4,5-trisphosphate.

Prior investigations relying on next-generation sequencing to detect genomic changes in post-resistance tumor samples from EGFR-TKI-treated patients have pinpointed several drivers, such as secondary EGFR mutations or amplification of MET or HER2 [5–8, 32]. Yet, in roughly half of instances, no clear mechanism emerges, pointing to non-genomic contributors like elevated levels of certain genes, proteins, or cytokines. While proinflammatory cytokines, particular immune subsets, and tumor-associated fibroblasts have been connected to EGFR-TKI failure [33–36], the exact ways these elements engage with EGFR-mutated malignant cells in patient tissues remain poorly defined. Our transcriptomic profiling of pretreatment EGFR-mutant NSCLC samples revealed IFITM3 as the sole transcript markedly elevated in cases with rapid progression (<12 months) versus prolonged control (>20 months) on osimertinib. Spatial gene expression mapping additionally demonstrated that tumor-cell IFITM3 rose due to inflammatory mediators primarily secreted by adjacent microenvironmental components following drug exposure. This crosstalk between the microenvironment and neoplastic cells could thus enhance malignant persistence via IFITM3 induction. Consequently, our methodology may uncover resistance pathways undetectable by standard genomic screening.

We further observed that malignant cells themselves secreted inflammatory mediators upon osimertinib challenge, aligning with earlier reports [15, 17, 36, 37]. Blockade of IL-6R or TNF-α curtailed the drug-triggered IFITM3 rise in NSCLC models, implying that this induction relies on autocrine/paracrine cytokine loops rather than direct EGFR inhibition. Spatial profiling also uncovered variable IFITM3 levels within single tumors, with local cellular composition analysis revealing no systematic variation in neighboring populations around IFITM3-high versus low neoplastic cells. Such intratumoral variability might therefore stem from differing cellular sensitivity to cytokines or uneven mediator distribution in the microenvironment.

Additional work is required to clarify cytokine-driven IFITM3 regulation and the origins of intratumoral signaling diversity.

Although PI3K-AKT hyperactivity has long been recognized in EGFR-TKI resistance [38–40], the triggers have stayed obscure. We now demonstrate that IFITM3 physically associates with MET to sustain AKT engagement, thereby fostering osimertinib tolerance. Disruption of lipid rafts diminished MET activation and reinstated drug responsiveness in IFITM3-high models. Considering IFITM3's reported role as a raft organizer that promotes B-cell receptor signaling in lymphoid malignancies [25], it may similarly serve as a platform to enable MET-PI3K coupling within rafts of EGFR-mutant lung cancer cells. Moreover, since heightened EGFR activity can stimulate JAK-STAT and IRF cascades [41, 42]—both established IFITM3 inducers [43–45]—IFITM3 could be central to sustaining viability in EGFR-driven tumors.

MET hyperactivity represents a classic acquired resistance route to EGFR-TKIs [46, 47], with genomic MET amplification detected in approximately 15% of osimertinib-resistant cases [48–50]. Both laboratory and patient data support dual EGFR/MET blockade to counter MET-dependent escape [51–55]. We reveal an alternative MET engagement mode: cytokine-elicited IFITM3 binding to MET during osimertinib therapy, yielding resistance. Concurrent MET inhibition blunted MET-AKT signaling and averted resistance emergence. These insights underscore the value of combining EGFR-TKIs with MET blockers not only to regain control in resistant settings but also to delay or prevent resistance onset in untreated EGFR-mutant NSCLC. Supporting this, adding the EGFR/MET-bispecific agent amivantamab to TKI regimens extended progression-free survival in this population [56].

Certain constraints apply to our work. Firstly, the postulated microenvironment–tumor interplay lacks direct in vivo confirmation. Humanized xenografts, patient-derived models, or organoid systems could better validate these dynamics. Secondly, we did not examine whether elevated IFITM3 coincides with established genomic resistance alterations. Thirdly, while IHC and spatial analyses linked IFITM3 induction to resistance progression, the limited paired clinical samples restrict broader conclusions. Larger prospective cohorts are essential to establish IFITM3 associations with specific resistance subtypes and to delineate precise microenvironment–malignant cell dialogues.

Conclusion

Overall, we uncover cytokine-mediated IFITM3 elevation—from both microenvironmental and autocrine sources—as a novel pathway driving acquired osimertinib resistance. Interfering with the IFITM3–MET interaction emerges as an attractive approach to enhance therapeutic success and circumvent IFITM3-associated resistance in EGFR-mutant NSCLC.

Acknowledgments: None

Conflict of Interest: None

Financial Support: None

Ethics Statement: None

References

1. Sung H, Ferlay J, Siegel RL, Laversanne M, Soerjomataram I, Jemal A, et al. Global cancer statistics 2020: GLOBOCAN estimates of incidence and mortality worldwide for 36 cancers in 185 countries. CA Cancer J Clin. 2021;71:209–49.
2. Kobayashi Y, Mitsudomi T. Not all epidermal growth factor receptor mutations in lung cancer are created equal: perspectives for individualized treatment strategy. Cancer Sci. 2016;107:1179–86.
3. Gazdar A. Activating and resistance mutations of EGFR in non-small-cell lung cancer: role in clinical response to EGFR tyrosine kinase inhibitors. Oncogene. 2009;28:S24–31.
4. Soria J-C, Ohe Y, Vansteenkiste J, Reungwetwattana T, Chewaskulyong B, Lee KH, et al. Osimertinib in untreated EGFR-mutated advanced non–small-cell lung cancer. N Engl J Med. 2018;378:113–25.
5. Planchard D, Loriot Y, Andre F, Gobert A, Auger N, Lacroix L, et al. EGFR-independent mechanisms of acquired resistance to AZD9291 in EGFR T790M-positive NSCLC patients. Ann Oncol. 2015;26:2073–8.
6. Taniguchi H, Yamada T, Wang R, Tanimura K, Adachi Y, Nishiyama A, et al. AXL confers intrinsic resistance to osimertinib and advances the emergence of tolerant cells. Nat Commun. 2019;10:259.
7. Ho CC, Liao WY, Lin CA, Shih JY, Yu CJ, Yang JC. Acquired BRAF V600E mutation as resistant

mechanism after treatment with osimertinib. J Thorac Oncol. 2017;12:567–72.
8. Piper-Vallillo AJ, Sequist LV, Piotrowska Z. Emerging treatment paradigms for EGFR-Mutant lung cancers progressing on osimertinib: A review. J Clin Oncol. 2020;38:2926–36.
9. Leonetti A, Sharma S, Minari R, Perego P, Giovannetti E, Tiseo M. Resistance mechanisms to osimertinib in EGFR-mutated non-small cell lung cancer. Br J Cancer. 2019;121:725–37.
10. Moghal N, Li Q, Stewart EL, Navab R, Mikubo M, D'Arcangelo E, et al. Single-cell analysis reveals transcriptomic features of drug-tolerant persisters and stromal adaptation in a patient-derived EGFR-mutated lung adenocarcinoma xenograft model. J Thorac Oncol. 2023;18:499–515.
11. Sun Y, Dong Y, Liu X, Zhang Y, Bai H, Duan J, et al. Blockade of STAT3/IL-4 overcomes EGFR T790M-cis-L792F-induced resistance to osimertinib via suppressing M2 macrophages polarization. EBioMedicine. 2022;83:104200.
12. Huang J, Lan X, Wang T, Lu H, Cao M, Yan S, et al. Targeting the IL-1beta/EHD1/TUBB3 axis overcomes resistance to EGFR-TKI in NSCLC. Oncogene. 2020;39:1739–55.
13. Wan X, Xie B, Sun H, Gu W, Wang C, Deng Q, et al. Exosomes derived from M2 type tumor-associated macrophages promote osimertinib resistance in non-small cell lung cancer through MSTRG.292666.16-miR-6836-5p-MAPK8IP3 axis. Cancer Cell Int. 2022;22:83.
14. Feng H, Cao B, Peng X, Wei Q. Cancer-associated fibroblasts strengthen cell proliferation and EGFR TKIs resistance through aryl hydrocarbon receptor dependent signals in non-small cell lung cancer. BMC Cancer. 2022;22:764.
15. Gong K, Guo G, Gerber DE, Gao B, Peyton M, Huang C, et al. TNF-driven adaptive response mediates resistance to EGFR inhibition in lung cancer. J Clin Invest. 2018;128:2500–18.
16. Gong K, Guo G, Panchani N, Bender ME, Gerber DE, Minna JD, et al. EGFR inhibition triggers an adaptive response by co-opting antiviral signaling pathways in lung cancer. Nat Cancer. 2020;1:394–409.
17. Ibusuki R, Iwama E, Shimauchi A, Tsutsumi H, Yoneshima Y, Tanaka K, Okamoto I. TP53 gain-of-function mutations promote osimertinib resistance via TNF-alpha-NF-kappaB signaling in EGFR-mutated lung cancer. NPJ Precis Oncol. 2024;8:60.
18. Patel SA, Nilsson MB, Yang Y, Le X, Tran HT, Elamin YY, et al. IL6 mediates suppression of T- and NK-cell function in EMT-associated TKI-resistant EGFR-mutant NSCLC. Clin Cancer Res. 2023;29:1292–304.
19. Ibusuki R, Yoneshima Y, Hashisako M, Matsuo N, Harada T, Tsuchiya-Kawano Y, et al. Association of thyroid transcription factor-1 (TTF-1) expression with efficacy of PD-1/PD-L1 inhibitors plus pemetrexed and platinum chemotherapy in advanced non-squamous non-small cell lung cancer. Transl Lung Cancer Res. 2022;11:2208–15.
20. Zhou Y, Zhou B, Pache L, Chang M, Khodabakhshi AH, Tanaseichuk O, et al. Metascape provides a biologist-oriented resource for the analysis of systems-level datasets. Nat Commun. 2019;10:1523.
21. Nakamura S, Shibahara D, Tanaka K, Kishikawa Y, Hashisako M, Nakatomi K, Nakagaki N, Kohno M, Azuma K, Ibusuki R et al. Spatial dynamics of the tumor microenvironment in emerging resistance to targeted therapy in EGFR-mutated NSCLC. Preprint at https://www.biorxivorg/content/101101/202502106 37543v1 .2025.
22. Ghandi M, Huang FW, Jane-Valbuena J, Kryukov GV, Lo CC, McDonald ER 3rd, Barretina J, Gelfand ET, Bielski CM, Li H, et al. Next-generation characterization of the cancer cell line encyclopedia. Nature. 2019;569:503–8.
23. Bailey CC, Huang I-C, Kam C, Farzan M. Ifitm3 limits the severity of acute influenza in mice. PLoS Pathog. 2012. https://doi.org/10.1371/journal.ppat.1002909.
24. Friedman RL, Manly SP, McMahon M, Kerr IM, Stark GR. Transcriptional and posttranscriptional regulation of interferon-induced gene expression in human cells. Cell. 1984;38:745–55.
25. Lee J, Robinson ME, Ma N, Artadji D, Ahmed MA, Xiao G, et al. IFITM3 functions as a PIP3 scaffold to amplify PI3K signalling in B cells. Nature. 2020;588:491–7.
26. Everitt AR, Clare S, Pertel T, John SP, Wash RS, Smith SE, et al. IFITM3 restricts the morbidity and mortality associated with influenza. Nature. 2012;484:519–23.
27. Poddar S, Hyde JL, Gorman MJ, Farzan M, Diamond MS. The Interferon-Stimulated gene

IFITM3 restricts infection and pathogenesis of arthritogenic and encephalitic alphaviruses. J Virol. 2016;90:8780–94.
28. Hur JY, Frost GR, Wu X, Crump C, Pan SJ, Wong E, Barros M, Li T, Nie P, Zhai Y, et al. The innate immunity protein IFITM3 modulates gamma-secretase in alzheimer's disease. Nature. 2020;586:735–40.
29. Xiong Z, Xu X, Zhang Y, Ma C, Hou C, You Z, et al. IFITM3 promotes glioblastoma stem cell-mediated angiogenesis via regulating JAK/STAT3/bFGF signaling pathway. Cell Death Dis. 2024;15:45.
30. Liu X, Chen L, Fan Y, Hong Y, Yang X, Li Y, Lu J, Lv J, Pan X, Qu F, et al. IFITM3 promotes bone metastasis of prostate cancer cells by mediating activation of the TGF-beta signaling pathway. Cell Death Dis. 2019;10:517.
31. Chu P-Y, Huang W-C, Tung S-L, Tsai C-Y, Chen CJ, Liu Y-C, et al. IFITM3 promotes malignant progression, cancer stemness and chemoresistance of gastric cancer by targeting MET/AKT/FOXO3/c-MYC axis. Cell Biosci. 2022;12:124.
32. Wu S-G, Shih J-Y. Management of acquired resistance to EGFR TKI–targeted therapy in advanced non-small cell lung cancer. Mol Cancer. 2018;17:1–14.
33. Wang S, Rong R, Yang DM, Fujimoto J, Bishop JA, Yan S, et al. Features of tumor-microenvironment images predict targeted therapy survival benefit in patients with EGFR-mutant lung cancer. J Clin Invest. 2023. https://doi.org/10.1172/JCI160330.
34. Han R, Guo H, Shi J, Wang H, Zhao S, Jia Y, Liu X, Li J, Cheng L, Zhao C, et al. Tumour microenvironment changes after osimertinib treatment resistance in non-small cell lung cancer. Eur J Cancer. 2023;189:112919.
35. Nilsson MB, Sun H, Diao L, Tong P, Liu D, Li L, et al. Stress hormones promote EGFR inhibitor resistance in NSCLC: implications for combinations with β-blockers. Sci Transl Med. 2017;9:eaao4307.
36. Li L, Han R, Xiao H, Lin C, Wang Y, Liu H, et al. Metformin sensitizes EGFR-TKI–resistant human lung cancer cells *in vitro* and *in vivo* through inhibition of IL-6 signaling and EMT reversal. Clin Cancer Res. 2014;20:2714–26.
37. Yao Z, Fenoglio S, Gao DC, Camiolo M, Stiles B, Lindsted T, et al. TGF-β IL-6 axis mediates selective and adaptive mechanisms of resistance to molecular targeted therapy in lung cancer. Proc Natl Acad Sci U S A. 2010;107:15535–40.
38. Jacobsen K, Bertran-Alamillo J, Molina MA, Teixido C, Karachaliou N, Pedersen MH, Castellvi J, Garzon M, Codony-Servat C, Codony-Servat J, et al. Convergent Akt activation drives acquired EGFR inhibitor resistance in lung cancer. Nat Commun. 2017;8:410.
39. Kim TM, Song A, Kim D-W, Kim S, Ahn Y-O, Keam B, et al. Mechanisms of acquired resistance to AZD9291: a mutation-selective, irreversible EGFR inhibitor. J Thorac Oncol. 2015;10:1736–44.
40. Terp MG, Jacobsen K, Molina MA, Karachaliou N, Beck HC, Bertran-Alamillo J, et al. Combined FGFR and Akt pathway inhibition abrogates growth of FGFR1 overexpressing EGFR-TKI-resistant NSCLC cells. NPJ Precis Oncol. 2021;5:65.
41. Yarden Y, Sliwkowski MX. Untangling the erbb signalling network. Nat Rev Mol Cell Biol. 2001;2:127–37.
42. Yamashita M, Chattopadhyay S, Fensterl V, Saikia P, Wetzel JL, Sen GC. Epidermal growth factor receptor is essential for Toll-like receptor 3 signaling. Sci Signal. 2012;5:ra50–50.
43. Honda K, Taniguchi T. IRFs: master regulators of signalling by Toll-like receptors and cytosolic pattern-recognition receptors. Nat Rev Immunol. 2006;6:644–58.
44. Lewin AR, Reid LE, McMAHON M, Stark GR, Kerr IM. Molecular analysis of a human interferon-inducible gene family. Eur J Biochem. 1991;199:417–23.
45. Schneider WM, Chevillotte MD, Rice CM. Interferon-stimulated genes: a complex web of host defenses. Annu Rev Immunol. 2014;32:513–45.
46. Engelman JA, Zejnullahu K, Mitsudomi T, Song Y, Hyland C, Park JO, et al. MET amplification leads to gefitinib resistance in lung cancer by activating ERBB3 signaling. Science. 2007;316:1039–43.
47. Yano S, Wang W, Li Q, Matsumoto K, Sakurama H, Nakamura T, et al. Hepatocyte growth factor induces gefitinib resistance of lung adenocarcinoma with epidermal growth factor receptor–activating mutations. Cancer Res. 2008;68:9479–87.
48. Yu HA, Arcila ME, Rekhtman N, Sima CS, Zakowski MF, Pao W, et al. Analysis of tumor specimens at the time of acquired resistance to EGFR-TKI therapy in 155 patients with EGFR-

mutant lung cancers. Clin Cancer Res. 2013;19:2240–7.

49. Leonetti A, Verze M, Minari R, Perrone F, Gnetti L, Bordi P, et al. Resistance to osimertinib in advanced EGFR-mutated NSCLC: a prospective study of molecular genotyping on tissue and liquid biopsies. Br J Cancer. 2024;130:135–42.
50. Chmielecki J, Gray JE, Cheng Y, Ohe Y, Imamura F, Cho BC, et al. Candidate mechanisms of acquired resistance to first-line osimertinib in EGFR-mutated advanced non-small cell lung cancer. Nat Commun. 2023;14:1070.
51. Xu L, Kikuchi E, Xu C, Ebi H, Ercan D, Cheng KA, et al. Combined EGFR/MET or EGFR/HSP90 inhibition is effective in the treatment of lung cancers codriven by mutant EGFR containing T790M and MET. Cancer Res. 2012;72:3302–11.
52. Sequist LV, Han JY, Ahn MJ, Cho BC, Yu H, Kim SW, Yang JC, Lee JS, Su WC, Kowalski D, et al. Osimertinib plus Savolitinib in patients with EGFR mutation-positive, MET-amplified, non-small-cell lung cancer after progression on EGFR tyrosine kinase inhibitors: interim results from a multicentre, open-label, phase 1b study. Lancet Oncol. 2020;21:373–86.
53. York ER, Varella-Garcia M, Bang TJ, Aisner DL, Camidge DR. Tolerable and effective combination of full-dose Crizotinib and osimertinib targeting MET amplification sequentially emerging after T790M positivity in EGFR-mutant non-small cell lung cancer. J Thorac Oncol. 2017;12:e85–8.
54. Gainor JF, Niederst MJ, Lennerz JK, Dagogo-Jack I, Stevens S, Shaw AT, Sequist LV, Engelman JA: Dramatic Response to Combination Erlotinib and Crizotinib in a Patient with Advanced, EGFR-Mutant Lung Cancer Harboring De Novo MET Amplification. J Thorac Oncol 2016, 11:e83-85.
55. Piotrowska Z, Isozaki H, Lennerz JK, Gainor JF, Lennes IT, Zhu VW, Marcoux N, Banwait MK, Digumarthy SR, Su W: Landscape of acquired resistance to osimertinib in EGFR-mutant NSCLC and clinical validation of combined EGFR and RET inhibition with osimertinib and BLU-667 for acquired RET fusion. Cancer discovery 2018, 8:1529-1539.
56. Cho BC, Lu S, Felip E, Spira AI, Girard N, Lee JS, Lee SH, Ostapenko Y, Danchaivijitr P, Liu B, et al. Amivantamab plus Lazertinib in Previously Untreated EGFR-Mutated Advanced NSCLC. N Engl J Med. 2024;391:1486–98.